A Search for Physics beyond the Standard Model

R.T. Jones
University of Connecticut, Storrs, CT
and
Jefferson Lab, Newport News, VA

July 10, 1997

Abstract

Parity violation in elastic electron scattering from hadronic targets provides a way to separate the weak neutral currents from the electromagnetic currents inside hadrons. Measurements of hadronic matrix elements of these weak neutral currents are beginning to provide important new information about nucleon structure by enabling the flavour-decomposition of quark vector matrix elements into separate contributions from up, down and strange quarks. Given measured values for the vector form-factors at intermediate values of Q^2, the Standard Model allows a precise prediction for their behaviour as $Q^2 \to 0$. Precise measurements of the parity-violating asymmetry in elastic scattering at forward angles and low-Q^2 would constitute a test of the Standard Model prediction, and provide a sensitive probe for certain kinds of New Physics. In this report a survey is made of the variety of targets of potential interest for Standard Model tests, and the experimental conditions are explored under which the desired precision might be attained.

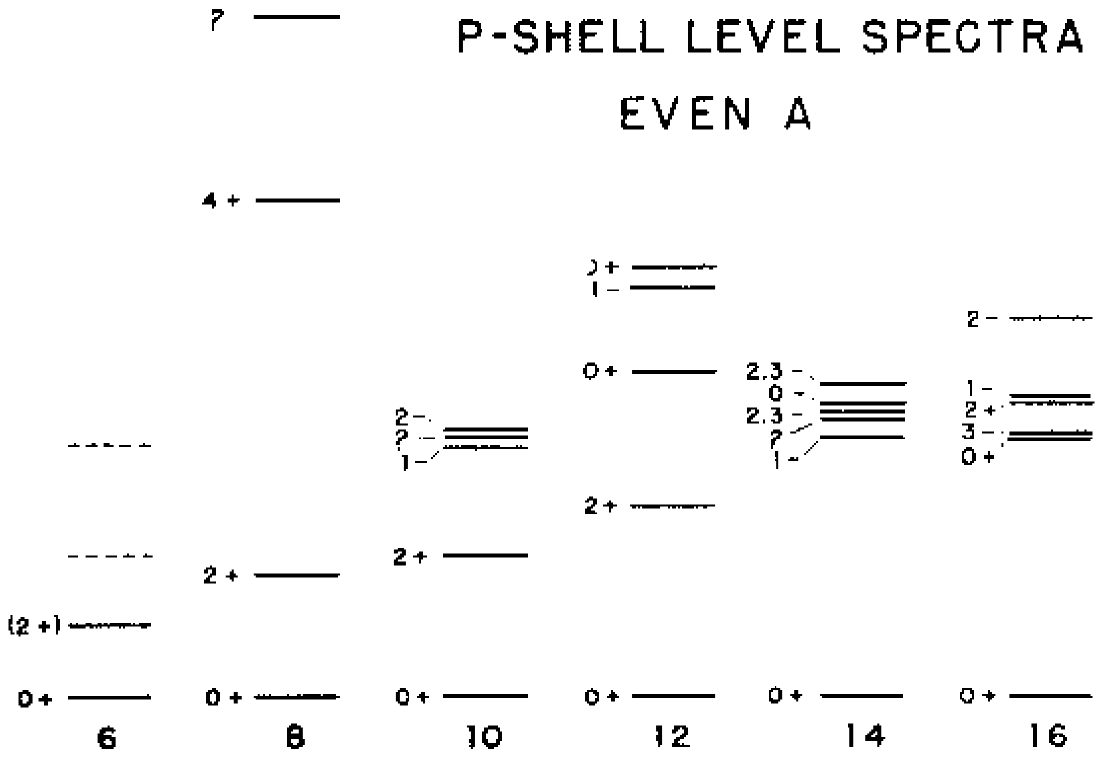

Figure 1: Spectrum of low-lying excited states of $J = 0$, $T = 0$ nuclei in the p-shell. The numbers along the bottom are atomic number A.

A search for physics beyond the Standard Model by measuring the parity-violating asymmetry in elastic electron scattering at intermediate energies has been identified[1] to be within the reach of experiments at CEBAF. In particular spin-0 isospin-0 nuclei in the low-A region are appropriate for these measurements because of the simple form nuclear current takes on in this case.

$$\left(\frac{\delta A}{A}\right)_{exp} = \left[\frac{1}{P^2\left(\frac{d\sigma}{d\Omega}\right) W\, L\, T\, A_{LR}^2} + \left(\frac{S_A}{A_{LR}}\right)^2\right]^{\frac{1}{2}}$$

Note that the dependence on the nuclear wave-function that is present in the Coulomb form factors F_{C0} cancel out in the ratio, leaving only the residual difference between the strangeness form factor and the electric isoscalar form factor intrinsic to the nucleon itself. The R_V factors carry the corrections to the tree-level Standard Model asymmetry. The goal of the experiment would be to measure $R_V^{(T=0)}$ as accurately as possible. The $\Gamma(q)$ factor contains corrections arising from the $T > 0$ admixture in the nuclear ground state, and is estimated to be at or below the 1% level for the nuclei studied below.

1 Survey of possible targets

In Fig. 1 is shown the nuclear level structure of the $J = 0$, $T = 0$ nuclei in the P-shell region. In order to separate elastic scattering from inelastic reactions, one would prefer a nucleus with the largest separation between the ground and the first excited states. Oxygen is the best candidate from this point of view, and also with regard to the cross section, which goes as Z^2. Carbon is also interesting because it makes for a simple and compact target, with good heat tolerance properties. Nuclei heavier than ^{16}O are less desirable

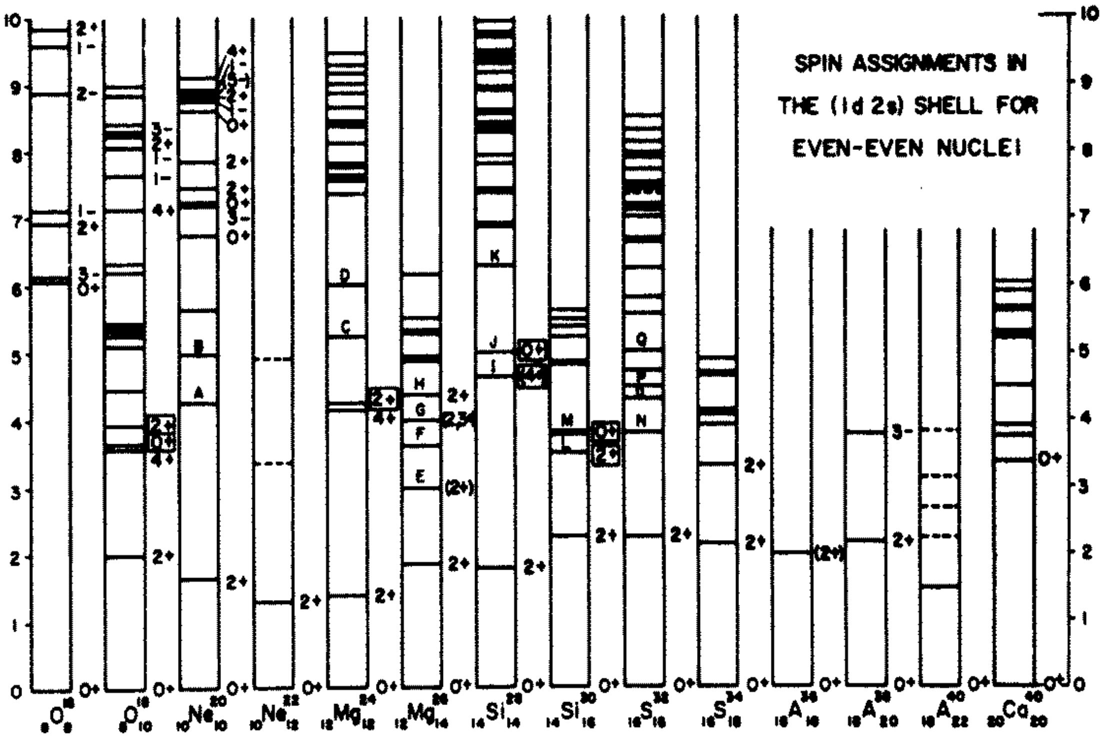

Figure 2: Spectrum of low-lying excited states of even-even nuclei in the sd-shell, showing the unique properties of ^{16}O in terms of its separation of the ground state from excited states.

from the point of view of low-lying excited states, as can be seen from Fig. 2. Also the ground states of nuclei beyond the p-shell contain increasing admixtures of T¿0 which complicate the interpretation of the data in terms of a Standard Model test.

The lightest 0+ nucleus is ^{4}He, which is interesting in spite of its low Z because of the simplicity of its excitation spectrum: it has no excited levels below 20MeV, which is where the continuum begins. In this study I concentrate on three specific targets, ^{16}O, ^{12}C and ^{4}He. Water is used for the oxygen target.

2 Water target

In all of the following figures is plotted lab scattering angle on the x-axis and colour is used to distinguish different electron beam energies. The Standard Model asymmetry for elastic scattering of polarized electrons from an ^{16}O target is shown in Fig. 3. These curves are calculated to leading order in the electroweak coupling, under the assumption that strange quarks do not contribute to the scattering of electrons from nuclei at these values of Q^2. The effect of a non-zero ρ_s is shown in Fig. 5. In Fig. 4 is shown the uncertainty in the measurement of the asymmetry for an experiment performed under the following assumptions.

1. luminosity $L = 10^{38}\text{cm}^{-2}\text{s}^{-1}$
2. duration $T = 1000\text{hr} = 3.6 \cdot 10^6\text{s}$
3. solid-angle $W = 0.01\text{sr}$
4. beam polarisation $P = 70\%$
5. systematic error on asymmetry $S_A = 10^{-8}$

Holding the solid angle fixed, the statistical error alone continues to decrease with decreasing scattering angle, regardless of the beam energy. This is because the cross section rises faster than A^2 is dropping as

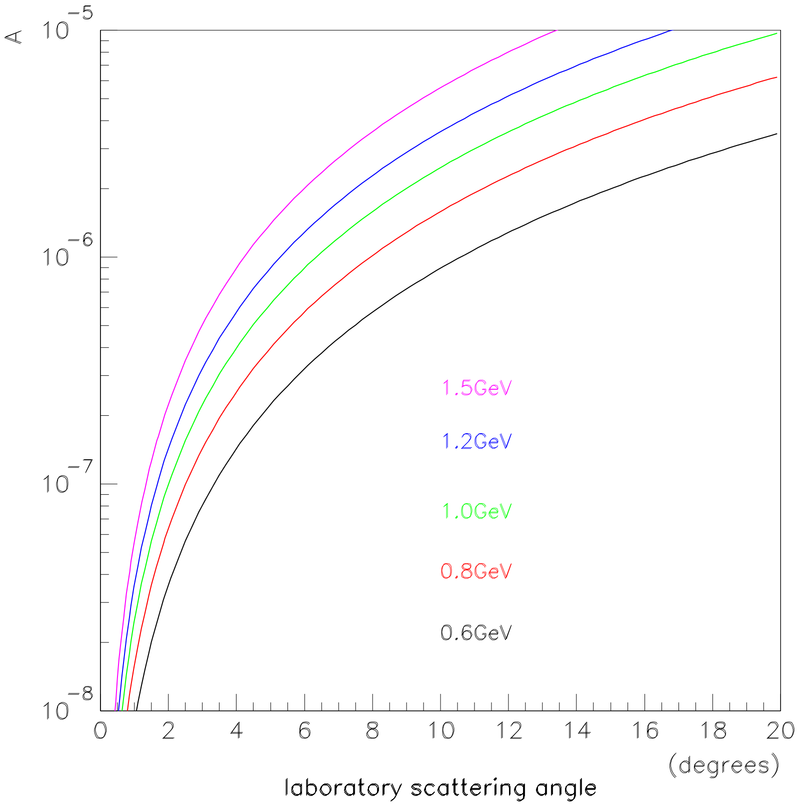

Figure 3: Standard Model asymmetry for elastic scattering of polarized electrons from ^{16}O *vs* lab scattering angle, for a variety of electron beam energies. The calculation assumes $\rho_s = 0$.

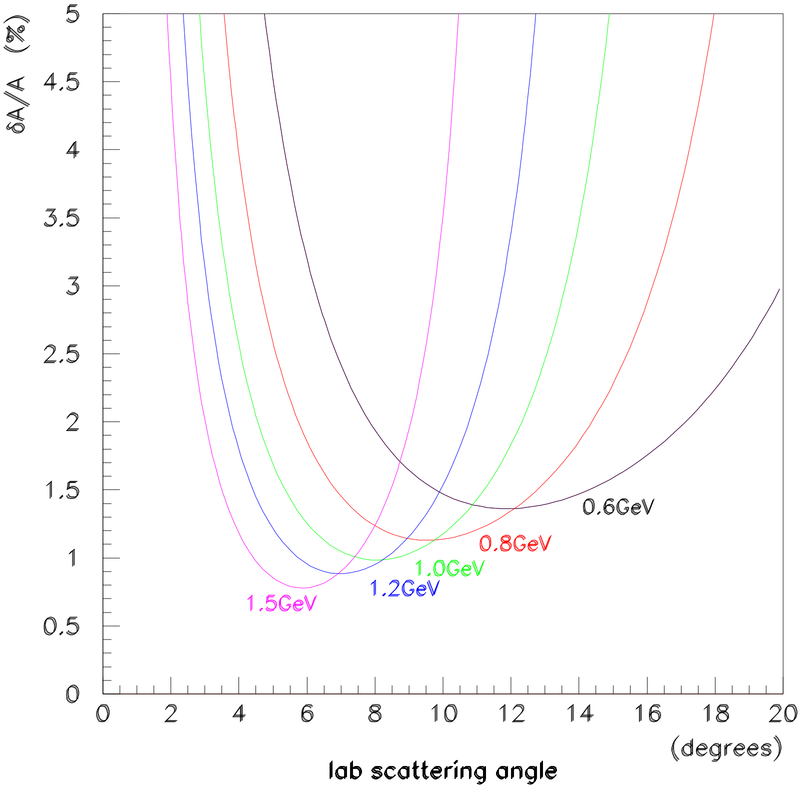

Figure 4: Percent uncertainty in the measured value of the asymmetry for ^{16}O under experimental conditions listed in the text, including statistical and systematic errors added in quadrature.

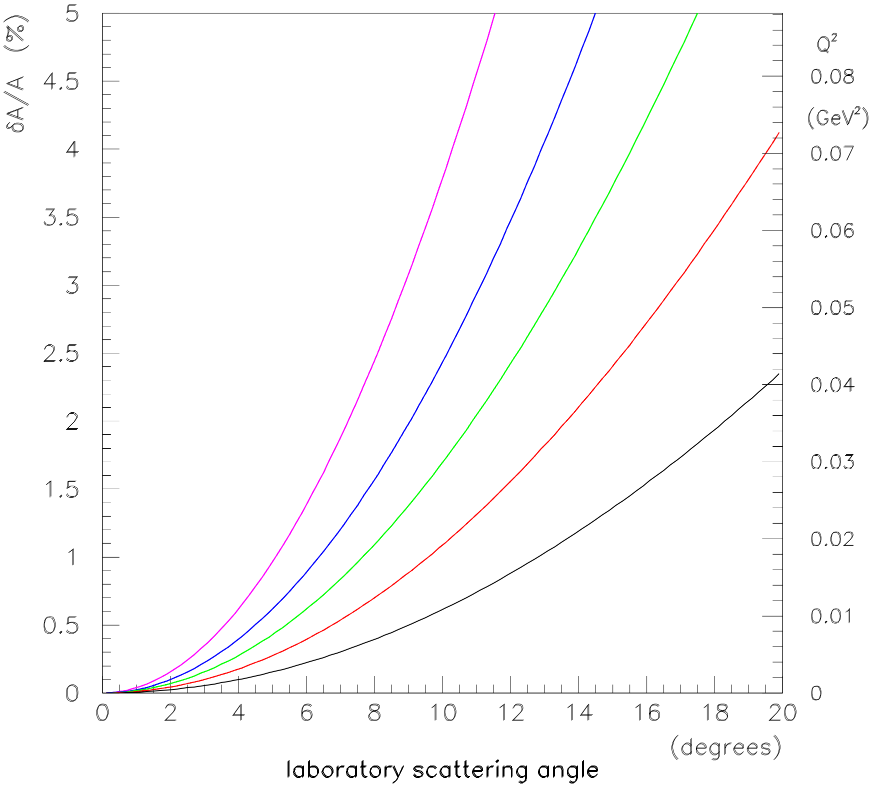

Figure 5: Contribution to the uncertainty in the measured asymmetry for ^{16}O arising from uncertainty in the value of ρ_s at the level of ± 1, for a variety of scattering angles and beam energies. The colour codes used to distinguish different beam energies are the same as used in Figs. 3-4.

one approaches zero degrees. However this does not take into account the inherent difficulties involved with controlling beam conditions well enough to measure very small differences in experimental rates. Even if the rates are high enough that statistical accuracy is not a problem, one must also insure that the magnitude of the asymmetry is large enough to measure under real experimental conditions. I take this into account by introducing into the experimental error a systematic uncertainty S_A as follows.

$$\left(\frac{\delta A}{A}\right)_{exp} = \left[\frac{1}{P^2\left(\frac{d\sigma}{d\Omega}\right) W\, L\, T\, A_{LR}^2} + \left(\frac{S_A}{A_{LR}}\right)^2\right]^{\frac{1}{2}}$$

The above figure of 10^{-8} for S_A is probably pessimistic for what is possible at CEBAF. The calculation will be repeated later with an order of magnitude lower systematic error.

To obtain an idea of what might stand in the way of comparing a measured asymmetry with the Standard Model value, I plot in Fig. 5 the percent uncertainty in A arising from the poorly known value of the strangeness radius of the nucleon ρ_s. For this figure I have taken ρ_s to be uncertain by ± 1, assuming that parity experiments presently underway will soon achieve this level of accuracy; at present there are no published measurements of ρ_s. Comparison with Fig. 4 shows that ρ_s would need to be experimentally constrained before one could reach the level of measuring electroweak corrections.

In Fig. 6 Figs. 4 and 5 are overlayed. This shows that running at higher energy increases the sensitivity to the strangeness form-factor. The best strategy for a Standard Model test might be to divide the running

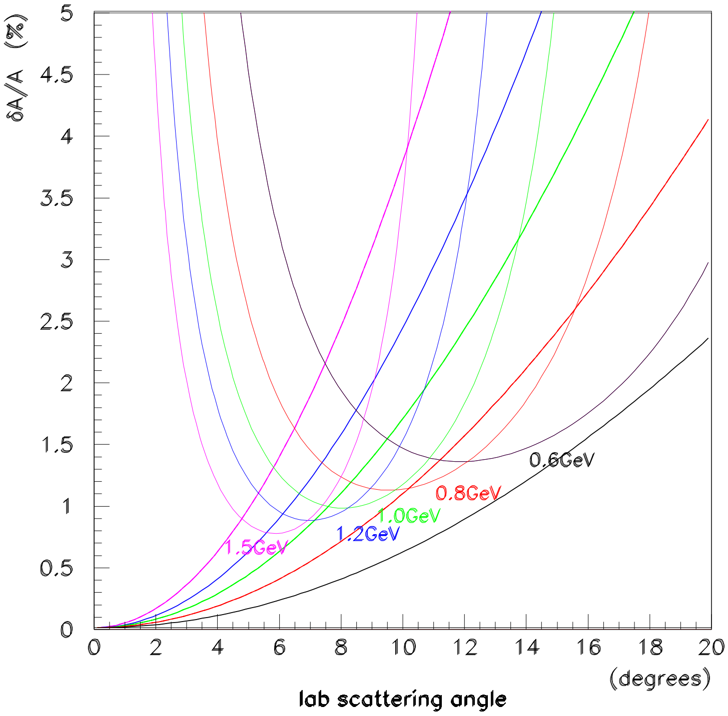

Figure 6: Overlay of Figs. 4 and 5 to show how the measurement accuracy on the asymmetry compares with the uncertainty in the Standard Model prediction that arises from ρ_s being known only to ± 1. In regions where the strangeness contribution is larger than the measurement error, the experiment constitutes a measurement of the strangeness form factor under Standard Model assumptions. In regions where the contribution from the strange form factor uncertainty is less than the measurement error, the experiment is able to test consistency between the data and the Standard Model, and place limits on possible new physics.

between high energy, to measure ρ_s, and low energy, where sensitivity to the residual uncertainty in ρ_s is minimised. To see how these result depend on the systematic error S_A the above calculation is repeated with $S_A = 10^{-9}$ and the results shown in Fig. 7. The optimum measurement angles move forward, as expected, and the experimental error on A for the conditions listed above improves somewhat. For an example of a running strategy, one might fix the spectrometer at 6^o in the lab and split the running between 1.5 (to measure ρ_s) and 600MeV to measure electroweak corrections.

So far we have only looked at ^{16}O; with a water target there would also be a contribution from hydrogen. A comparison of the cross section for electron scattering from ^{16}O and ^{1}H can be seen in Fig. 8. The cross sections are multiplied by q^4 to facilitate the comparison at low angles. The Standard Model asymmetry for the proton is shown in Fig. 9. In principle there are contributions from the strange quarks involving both ρ_s and μ_s, but these are poorly known at present and have been left out of the calculation.

The precision with which the proton asymmetry can be measured under the above experimental conditions is shown in Fig. 10 assuming a systematic error $S_A = 10^{-9}$. A measurement on hydrogen is not really feasible with a water target because there would be many more quasi-elastic than free proton events, and the two have a large kinematical overlap. Fig. 10 shows that the proton asymmetry is best measured at high energy, in distinction to the case of the $T = 0$ nucleus, where one wants to run with electrons in the vicinity of 1GeV.

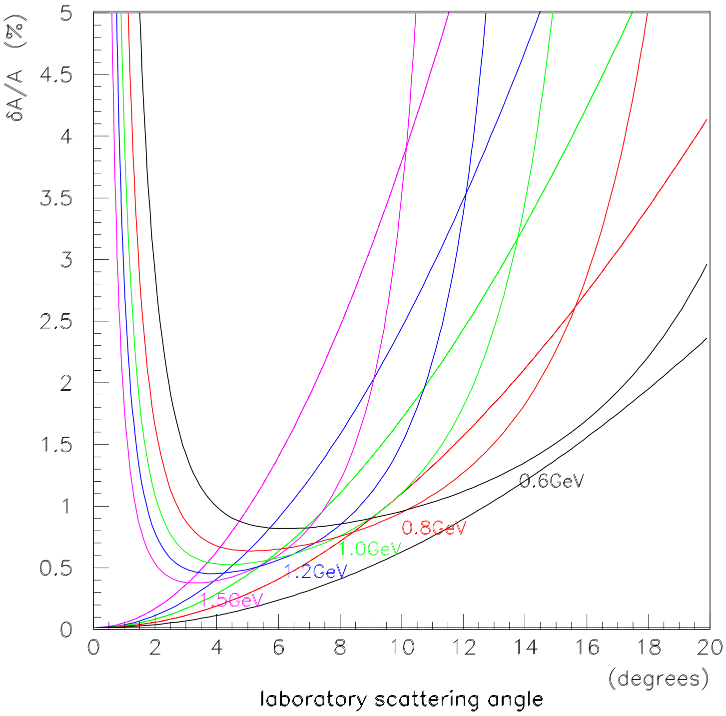

Figure 7: Same as Fig. 6 except that the systematic error $S_A = 10^{-9}$ has been used instead of $S_A = 10^{-8}$. The colour coding is the same as in Figs. 3-6.

1

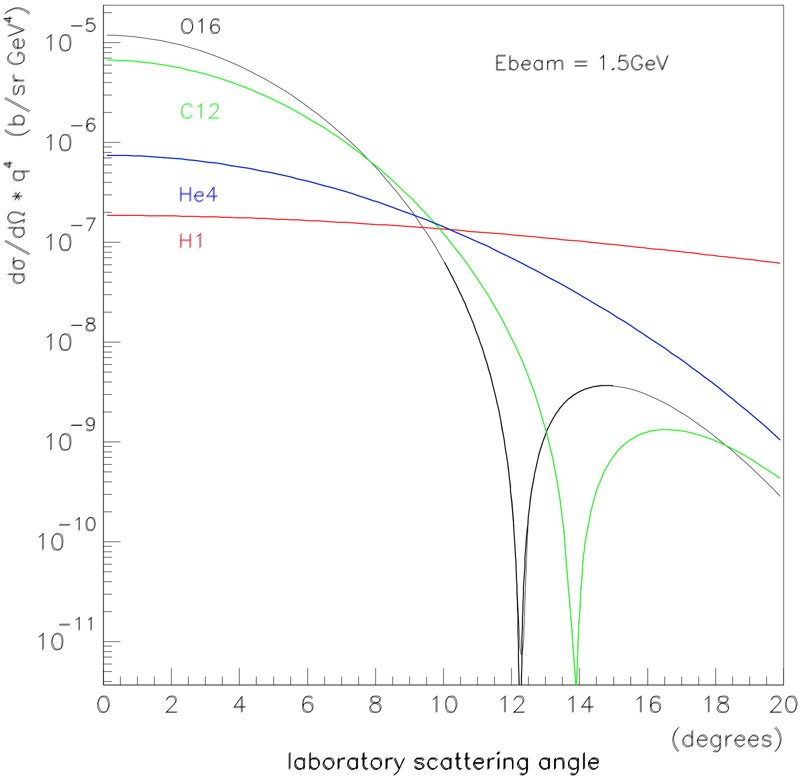

Figure 8: Differential cross section for elastic electron scattering from several targets at a beam energy of 1.5GeV. The factor q^{-4} in the Mott cross section has been suppressed to facilitate comparison at low Q^2.

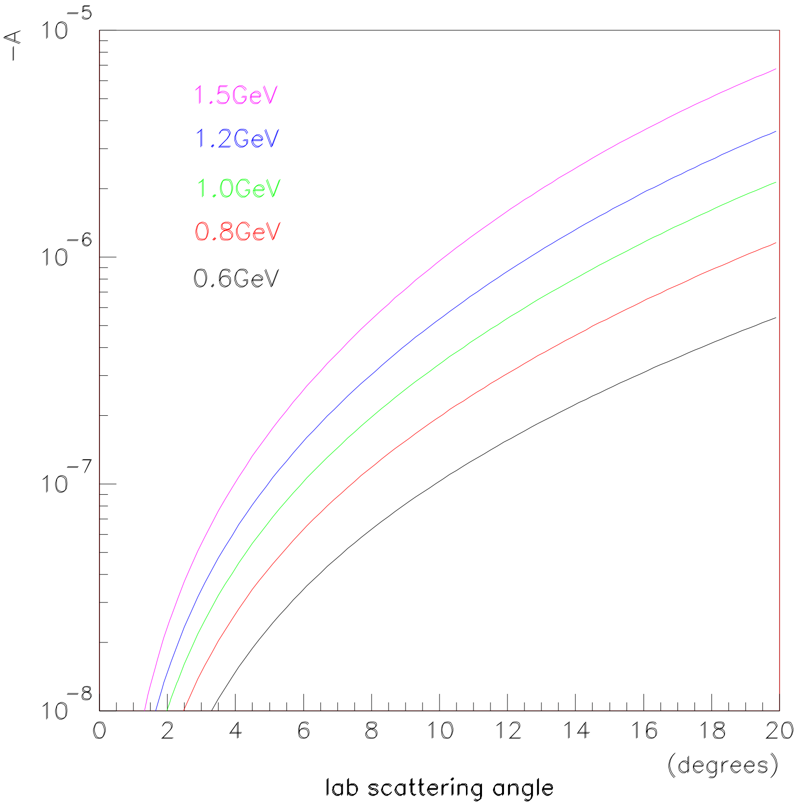

Figure 9: Standard Model asymmetry for elastic scattering of polarized electrons from the proton *vs* lab scattering angle, for a variety of electron beam energies. The calculation assumes $\rho_s = 0$ and $\mu_s = 0$.

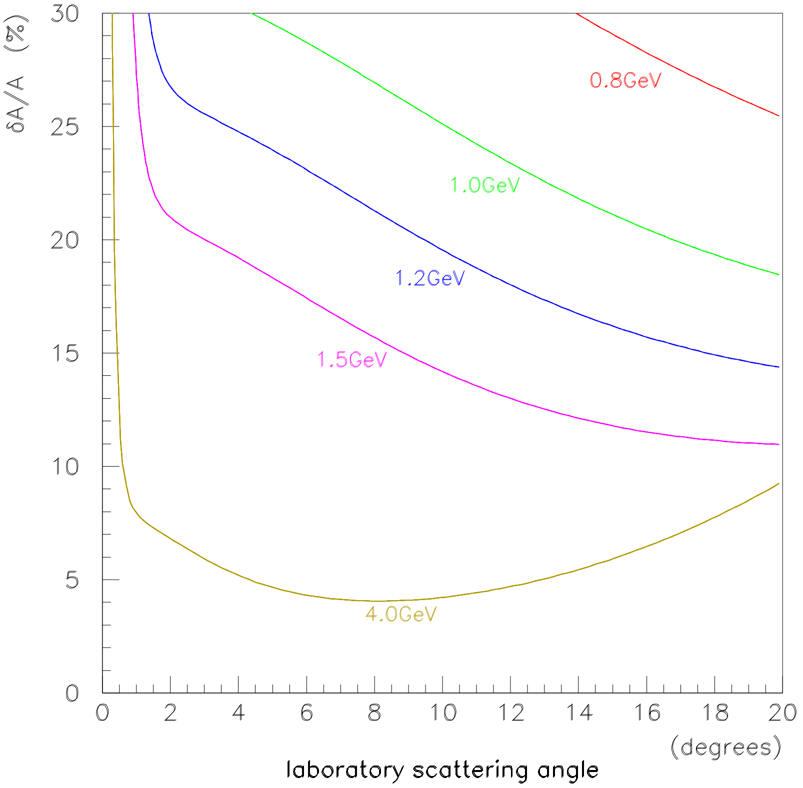

Figure 10: Percent uncertainty in the measured value of the asymmetry for ^{1}H under experimental conditions listed in the text, including statistical and systematic errors added in quadrature.

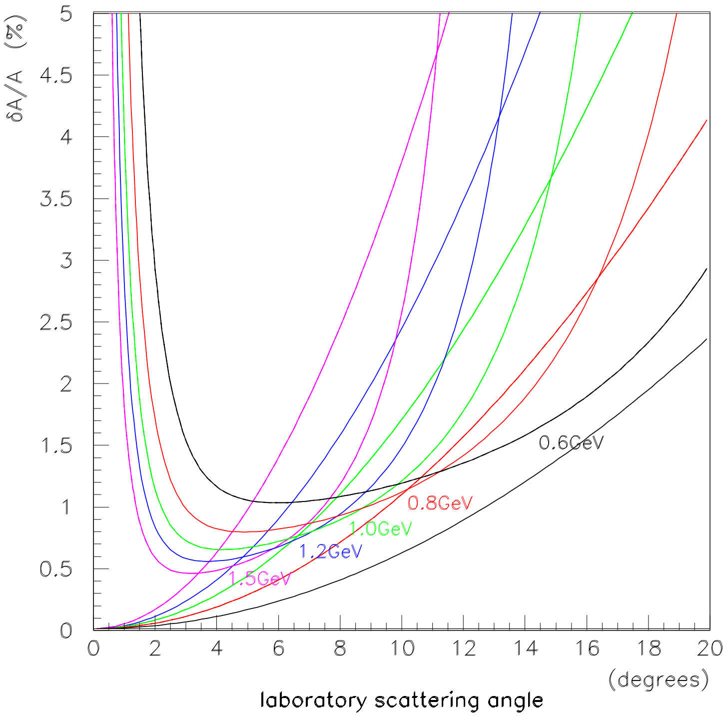

Figure 11: Same as Fig. 6, for a ^{12}C target instead of ^{16}O. A systematic error $S_A = 10^{-9}$ was used. The colour coding is the same as in Figs. 3-6.

3 Carbon target

In Fig. 11 is shown the experimental error on the asymmetry measurement with a the systematic error kept at $S_A = 10^{-9}$. It appears that the error for carbon is about 25% larger than that obtained with an oxygen (water) target of the same thickness in nuclei/cm^2. For the purposes of comparison between different nuclear targets, the experimental luminosity, and hence target thickness in nuclei/cm^2, are kept the same.

1

4 Helium target

Fig. 12 shows the same quantity calculated using a helium target, all other things kept the same. It appears that one does not gain in experimental precision at any energy or angle by going down from ^{16}O to lighter nuclei. The cross section is dropping fast enough that one is always confined to very forward angles to reach the desired statistical precision. Of all 0^+ targets, helium has the largest cross section from $Q^2 = 0.1$ GeV^2 and greater. This makes it the best target for measuring ρ_s. This measurement might be made at an intermediate value of Q^2, for example with a forward-scattering experiment at a beam energy 2-3GeV, and then the value used in the interpretation of data taken below 1GeV where the contribution from the strangeness form-factor to the total asymmetry is smaller and the results are sensitive to the electroweak radiative corrections.

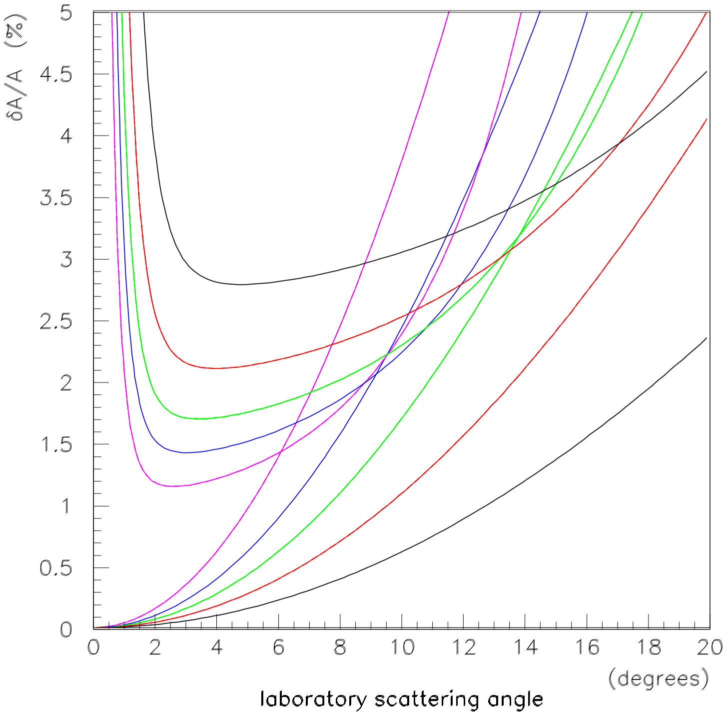

Figure 12: Same as Fig. 6, for a ^{4}He target instead of ^{16}O. A systematic error $S_A = 10^{-9}$ was used. The colour coding is the same as in Figs. 3-6.

1

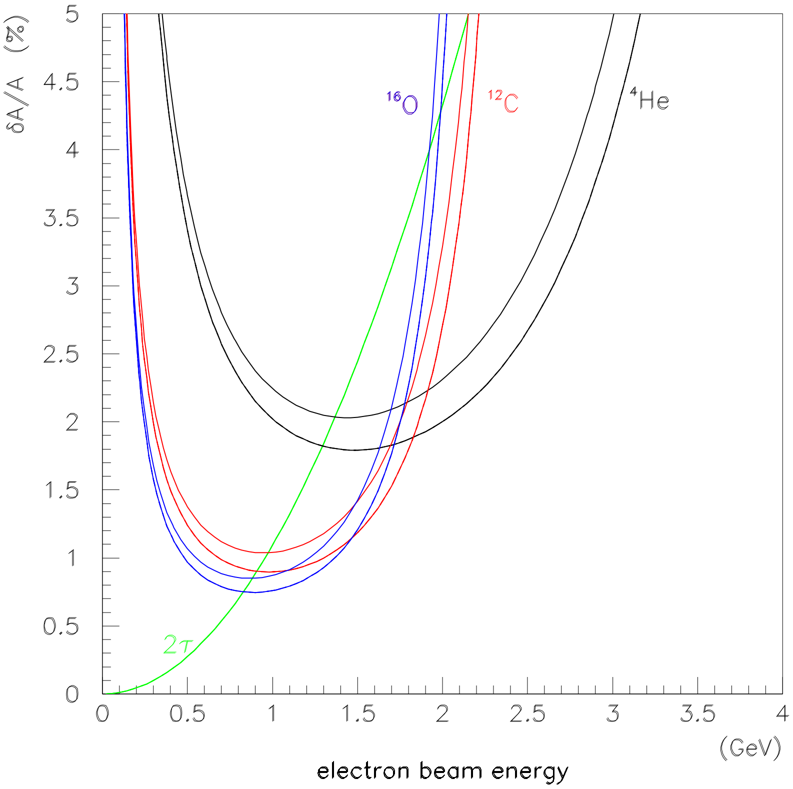

Figure 13: Percent measurement error on the asymmetry for a fixed scattering angle $\theta_{lab} = 8^o$ for the three $o^+T = 0$ targets under study. The lower curve in each pair is the same data as shown in Figs. 7, 11-12 but now plotted *vs* energy instead of scattering angle. The green curve indicates the Standard Model error on the asymmetry from an error in the strangeness radius of ± 1. The upper curve in a pair results from throwing away the part of the radiative tail of the elastic peak starting at the the first excited level (or continuum in the case of helium) of the recoil nucleus.

5 Comparison of three targets

These results show that in general one would like to measure the asymmetries at angles in the interval 5^o-8^o in the lab. In the conditions above we also assumed a solid-angle of 0.01sr. If I assume a spectrometer pair with approximately equal acceptance is symmetric in θ_x and θ_y, this translates to an area of roughly 4^o x 4^o on the unit sphere. If to maintain this acceptance we have to accept a 4^o bite in lab scattering angle, then it should be over the range 6^o - 10^o, or centred at 8^o. Since this is more or less independent of energy and target, I henceforth fix the scattering angle at 8^o and plot measurement error *vs* beam energy. All three 0^+ T=0 targets are shown together in Fig. 13. The lower curve in each pair is the same data as shown in Figs. 7,11-12 but now plotted *vs* energy instead of scattering angle. The green curve indicates the contribution to the error on the asymmetry from an error in the strangeness radius of ± 1. The upper curve in a pair results from throwing away the part of the radiative tail of the elastic peak starting at the the first excited level (or continuum in the case of helium) of the recoil nucleus. Such a cut would be necessary in order to separate the elastic from inelastic scattering.

In addition to nuclear excited states, with a water target one must also be concerned at some level with separating out the contribution of scattering from the free protons. The following simplified picture of the

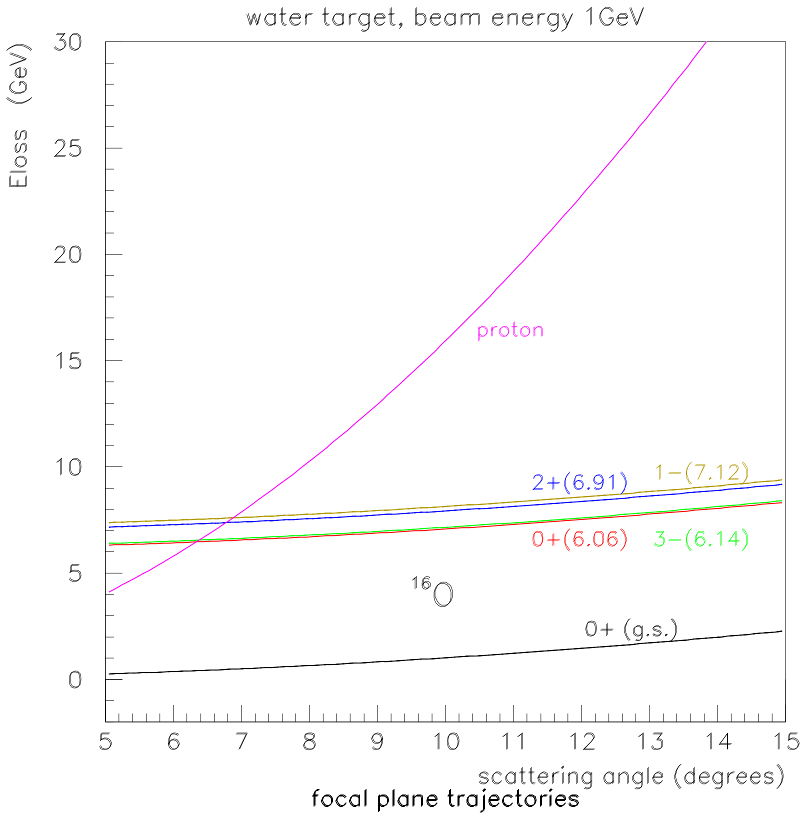

Figure 14: Focal plane trajectories for elastic scattering of 1GeV electrons from ^{16}O (black) and ^{1}H (purple) for a water target. The trajectories for inelastic scattering to the lowest-lying excited states of ^{16}O are shown in other colours.

focal plane serves to illustrate the kinematic separation between the two elastic peaks as a function of angle. At a beam energy of 1GeV the proton lies beyond the excited nuclear levels for most of the accessible angular range, and would be eliminated by the same cut that separates elastic from inelastic scattering from ^{16}O. But at 600MeV the separation is less clear, as shown in Fig. 15. However at these low values of Q^2 the cross section for ^{1}H is a factor of 50 less than ^{16}O (see Fig. 8) and the asymmetry of the proton is an order of magnitude less than for oxygen, so the effect is small and easily corrected for at low Q^2. The same is not true at higher values of Q^2, as one approaches the the diffraction minimum for ^{16}O, where hydrogen would dominate the asymmetry. But there the kinematic separation on the focal plane is also large, so there would be no confusion between the two. The conclusion is that the presence of hydrogen in water nowhere diminishes its effectiveness as an oxygen target.

The outcome of this preliminary comparison is that ^{16}O in the form of water provides the best target for a precision measurement of the weak isoscalar charge of the nucleon. As was already shown by Donnelly *et.al.*[1] it is possible, within parameters accessible for an experiment at CEBAF, to make a 1% measurement of this charge which would be competitive with the limits currently established by atomic parity-violation experiments. However there are still some practical questions that have to be addressed for an experiment that would like to run at a luminosity of 10^{38}cm-2s^{-1}.

1. How does the use of a thick target affect the ability to resolve elastic from inelastic scattering?

2. What are the practical limits on luminosity that arise from the power dissipation requirements for each

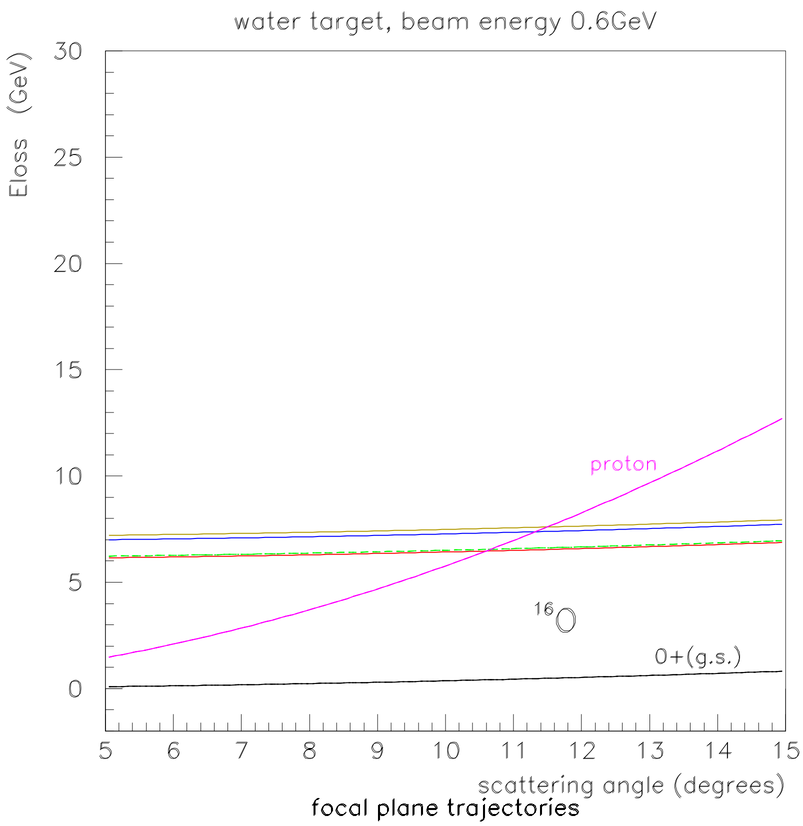

Figure 15: Same as Fig. 14 for electron beam energy reduced to 600MeV.

Table 1: Target thickness, for each of the target materials, corresponding to a luminosity of $10^{38}\mathrm{cm}^{-2}\mathrm{s}^{-1}$ and 100μA of beam current.

	target length (cm)	radiation length (cm)	target length (% rad.len.)
water	4.9	36.1	13.6
carbon	1.4	18.8	7.4
helium (liquid)	8.6	756	1.1

type of target?

3. Can any of the existing spectrometers at CEBAF operate at angles forward of 10^o with an acceptance of 0.01sr and still obtain the necessary separation between the elastic and inelastic channels? What limits does this place on target length?

The first of these considerations is taken up in detail in the remaining body of this report. The second is covered in a preliminary way in Appendix A. It requires further study once a clear choice has emerged for the target material. The third is independent of target type and requires the selection of a particular spectrometer to be adapted to the needs of this experiment. Appendix B outlines some work underway in this regard.

6 Thick target effects

The benchmark luminosity used by Donnelly *et.al.*[1] of $10^{38}\mathrm{cm}^{-2}\mathrm{s}^{-1}$ translates into the target thickness shown in Table 1 for each type of target, assuming a beam current of 100μA. The two effects related to resolution that arise when considering targets as thick as $0.1X_0$ are external bremsstrahlung and multiple scattering in the target.

6.1 internal bremsstrahlung

I use the term *internal bremsstrahlung* to refer to the Q.E.D. radiative corrections that are associated with the primary scattering event. This is not a thick-target effect, and was already introduced in Fig. 13, but is described here to make clear its distinction from *external bremsstrahlung* discussed in the next section. The correction to the elastic scattering cross section due to internal bremsstrahlung is contained in the logarithmic term of the following n.l.o. elastic scattering cross section.

$$\begin{aligned} \left(\frac{d\sigma}{d\Omega}\right)_{\mathrm{elastic}} &= \left(\frac{d\sigma}{d\Omega}\right)_{\mathrm{Mott}} \left[1 - \frac{2\alpha}{\pi} \ln\left(\frac{E}{E_{\mathrm{cut}}}\right) \chi(Q^2)\right] \\ \chi(Q^2) &\xrightarrow{Q^2 \gg m_{\mathrm{e}}^2} \ln\left(\frac{Q^2}{m_{\mathrm{e}}^2}\right) - 1 \end{aligned}$$

The magnitude of the correction depends on E_{cut} where one cuts off the radiative tail of the scattered electron energy distribution. The requirement the the experiment discriminate between elastic and inelastic scattering fixes an upper limit for E_{cut} for each type of target, which I take to be 6MeV for water, 4MeV for carbon, and 20MeV for helium. The exact values do not matter very much because they only enter the cross section through a logarithm. Under these conditions there is a reduction in the cross section of about 30% for all three targets due to internal bremsstrahlung. This is represented by the difference between the two curves in each colour in Fig. 13. This correction is independent of target thickness.

6.2 external bremsstrahlung

There is another effect, also classed as a radiative correction, which does depend on target thickness, which I call *external bremsstrahlung*. This has to do with radiation that occurs in a separate scattering event from the primary one. The incoming electron may radiate some energy through a prior interaction in the target before it undergoes the primary collision, or the radiation may occur after the primary scattering event; the effect is the same. The problem is actually more complicated than simply considering just these two cases. The energy-loss distribution due to bremsstrahlung rises like $1/k$ as $k \to 0$, with the result that for any finite target thickness there is a certain energy scale below which multiple-radiation effects become important and one can no longer consider just single-photon radiative corrections. This is true for all target thicknesses; however, for very thin targets the scale can be pushed far into the infrared, leaving single-photon corrections dominant at energy scales that are relevant to the problem. Here we are interested in effects that are important at the MeV scale.

For the bremsstrahlung spectrum I take the following simplified formula, which has the correct infrared behaviour, the right average radiation rate (if x is measured in radiation lengths) and cuts off at the endpoint.

$$\left(\frac{d^2N_\gamma}{dk\,dx}\right)_{\text{brems}} = 2\left(\frac{1}{k} - \frac{1}{E}\right)$$

I now divide the target up into n slices along the incident beam direction and apply this formula for the energy loss K-distribution of the electron as it traverses each layer. Since we are considering targets much less than X_0 thick and are only interested in the distribution near the peak, I use the incident electron energy of 1GeV for E in all of the layers. In this case the distribution $g(K)$ for electrons emerging from the target is given by

$$g(K) = e^{2\lambda}\left(\frac{E_{\text{cut}}}{E}\right)^{2\lambda}\left[g_0(K) + \frac{2\lambda}{n}\left(\frac{1}{K} - \frac{1}{E}\right)\right]^{(n)}$$

where the exponent (n) refers to auto-convolution n times. I take the incident beam lineshape $g_0(K)$ to be a delta function for our purposes. This function is normalised to unity and has the correct mean energy loss in the limit of large n. This convolution is best carried out numerically. I carried it out for this study with $n = 1000$, although for these target thicknesses convergence was obtained already with $n = 100$. In Fig. 16 is shown the energy profile for a 1GeV incident electron exiting from a target of 1% radiation length, in the vicinity of the peak. Zero in this plot corresponds to a 1GeV transmitted electron, 0.01 to a 0.990GeV electron, and so on. The vertical axis is probability normalised to 1 over the whole spectrum out to 1GeV. For this case most of the beam remains in the first bin, that is, within 1MeV of the incident beam energy. For a target of 0.1 radiation lengths or larger, as shown in Fig. 17, the first bin no longer contains the majority of the scattered beam.

To apply these results to the problem at hand, I assume that a measurement at low angles requires a disk target geometry where the scattered and unscattered beam traverse essentially the same thickness of target. This means that no matter where inside the target the primary scattering occurs, the electron must traverse the same amount of target material on the way to the detector. An exception to this assumption will be considered later in the case of an extended helium target. Integrating the probabilities in Figs. 16-17 up to E_{cut} gives the fraction of the elastic scattering events that enter into the measured elastic peak at the detector. This can be multiplied by the target thickness to yield an *effective target thickness*, that is, the equivalent amount of target that contributes to the measurable elastic cross section. This is shown for three different values of E_{cut} in Fig. 18. Note that these curves apply to any target material as long as thickness is measured in radiation lengths.

These results show

1. that there is a limit to the useful luminosity that one can obtain for a given beam current and target material, that turns out to be on the order of 5% rad.len., and

2. that there is an optimum target thickness that yields the maximum usable luminosity for elastic scattering, which depends somewhat on the elastic cutoff, but is on the order of 10% rad.len.

To explore what ramifications this might have for the experiment in question, I now re-evaluate in Table 2 the usable luminosity for each type of target under optimal conditions.

These are reasonable thicknesses for physical targets, except for the case of the 1.1m helium target. There are several reasons why a target more than 1m long is a difficulty, not the least of which is the considerable amount of power that would have to be dissipated by the cryogenics. This matter is taken up again in the

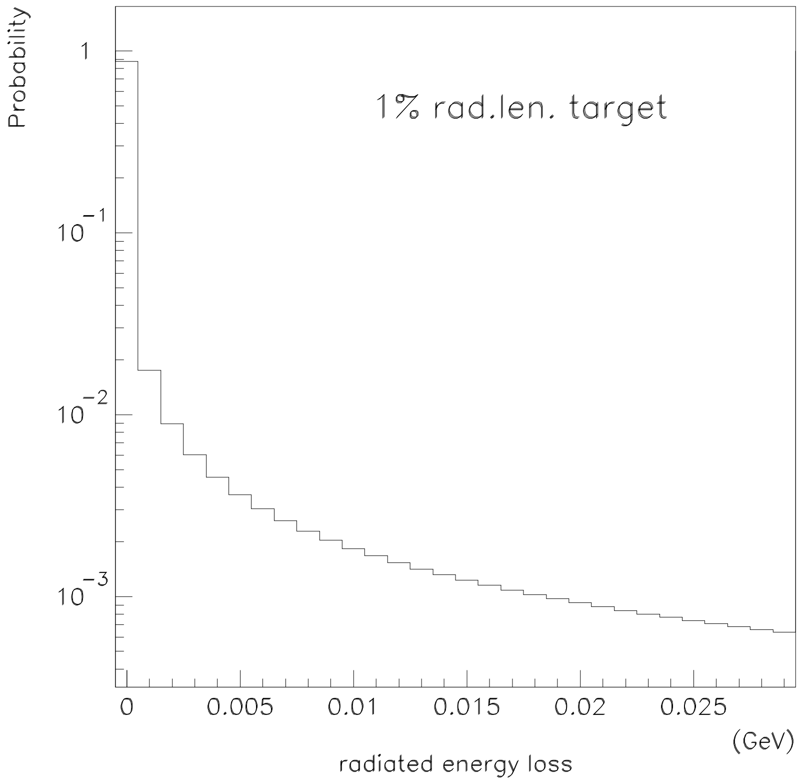

Figure 16: Radiative energy loss spectrum for a 1GeV electron incident on a target of 1% radiation length.

Table 2: Effective luminosity that contributes to the measured signal for a 100μA electron beam and target thickness optimised for maximum rate within the elastic scattering window.

	cutoff (MeV)	max. eff. target thickness (% rad.len.)	phys. target thickness (cm)	eff. luminosity (10^{38}cm^{-2}s^{-1})
^{16}O (water)	6	4.5	4.3	0.33
^{12}C (graphite)	4	4.2	2.1	0.57
^{4}He (liquid)	20	5.9	113	5.4
^{4}He (short)	20	1.6	12.5	1.35

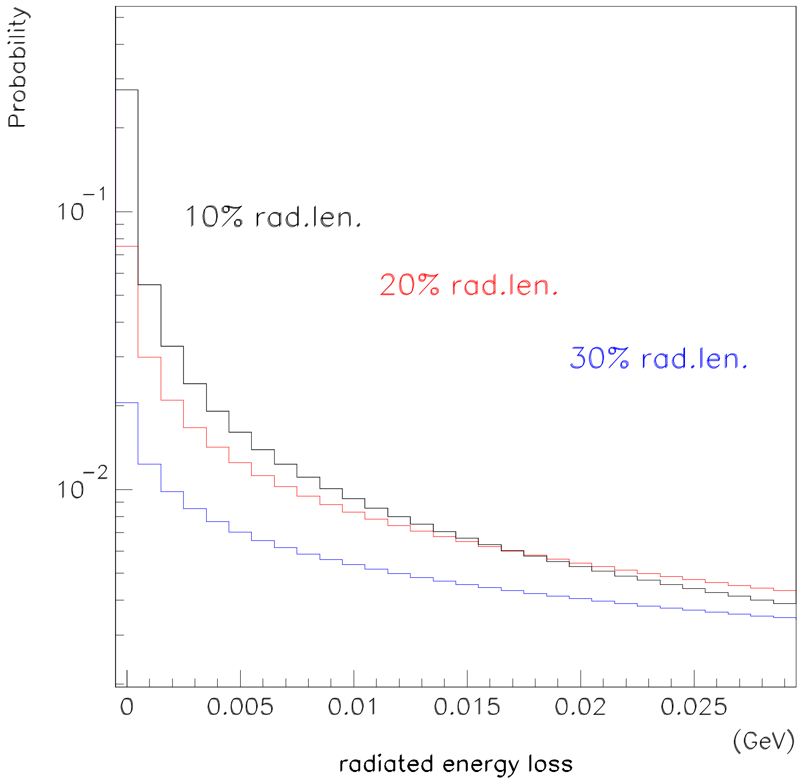

Figure 17: Radiative energy loss spectrum for a 1GeV electron incident on a target of 1% radiation length.

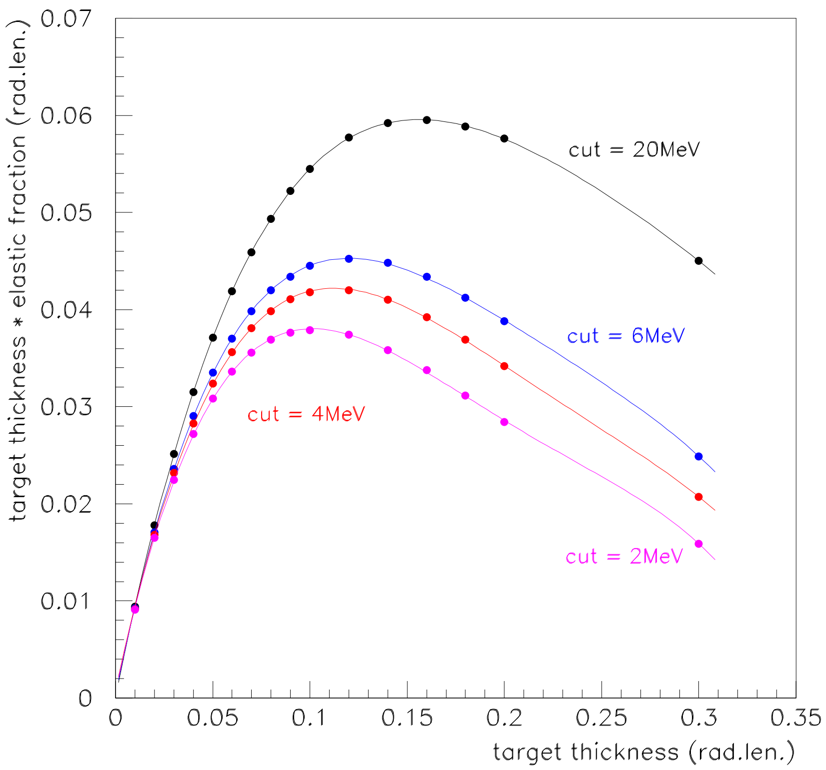

Figure 18: Effective target thickness *vs* physical target thickness for different values of $E_{\rm cut}$. The reduction from actual to effective target thickness is due to external bremsstrahlung of photons with energy greater than $E_{\rm cut}$.

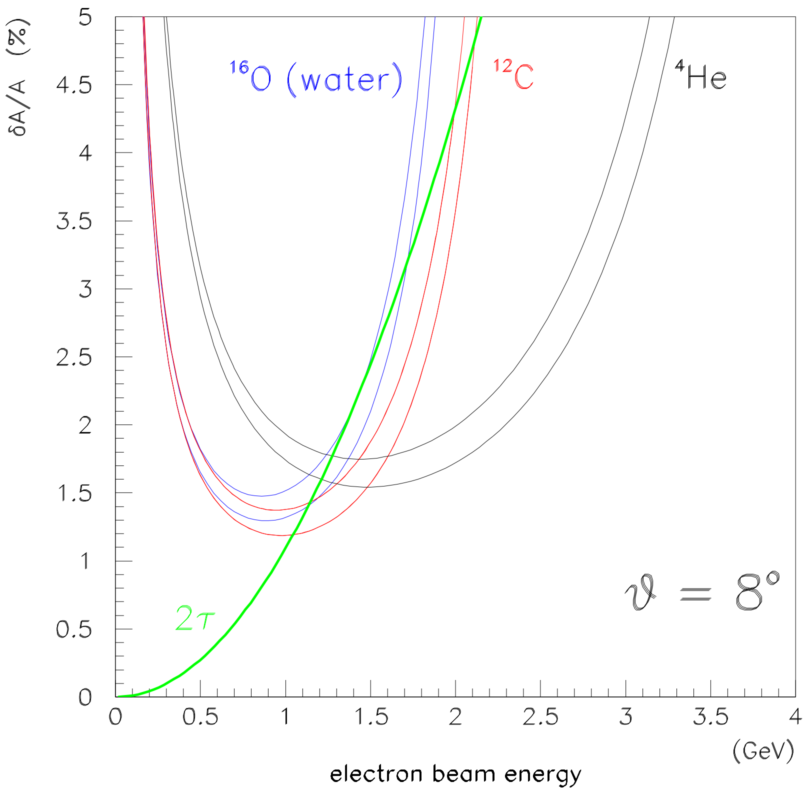

Figure 19: Percent error on the measured asymmetry *vs* electron beam energy fixed at 8^o lab scattering angle, after correcting for losses from external bremsstrahlung (lower curve of each pair) and both external and internal bremsstrahlung (upper curve of each pair). The Standard Model error arising from a ± 1 uncertainty in ρ_s is superimposed in green.

next section. For the present purposes, I consider a 12.5cm (300W) target to be within the limits of what is practical, and proceed with the comparison on this basis. The parameters for such a target are shown in the last line of Table 2.

I now repeat the calculation of the experimental error on the measured asymmetry, using the corrected values for the effective luminosity for each target. As before, the upper curve in each colour is the more important one, as it contains the cross section that one would actually measure inside the elastic window. Now all three targets are quite close to one another in the ultimate limits of their precision, although they differ somewhat in the kinematics where the optimum precision is reached. Carbon has edged out water by a small margin as the best target from the point of view of absolute precision.

Just as an exercise, I set aside questions of technical feasibility and spectrometer optics, and consider what the ultimate limits would be with a 1m helium target. This is shown in Fig. 20. Both this and the preceding figure are evaluated assuming a systematic error $S_A = 10^{-9}$. In the case of an extended target like this, it is no longer valid to consider that all of the electrons traverse the full thickness of the target. If the target were in the form of a tube of transverse dimensions only a few cm then the electrons would exit the target not far downstream of the primary vertex, giving the effect of a thinner target. They would, however, have to penetrate the walls of the target vessel at rather low angles, which would restore a part of the losses. For this study I assumed an aluminium target vessel with walls 300μm thick, and recalculated the elastic yield. The calculation took into account the fact that a greater number of the detected elastic events come

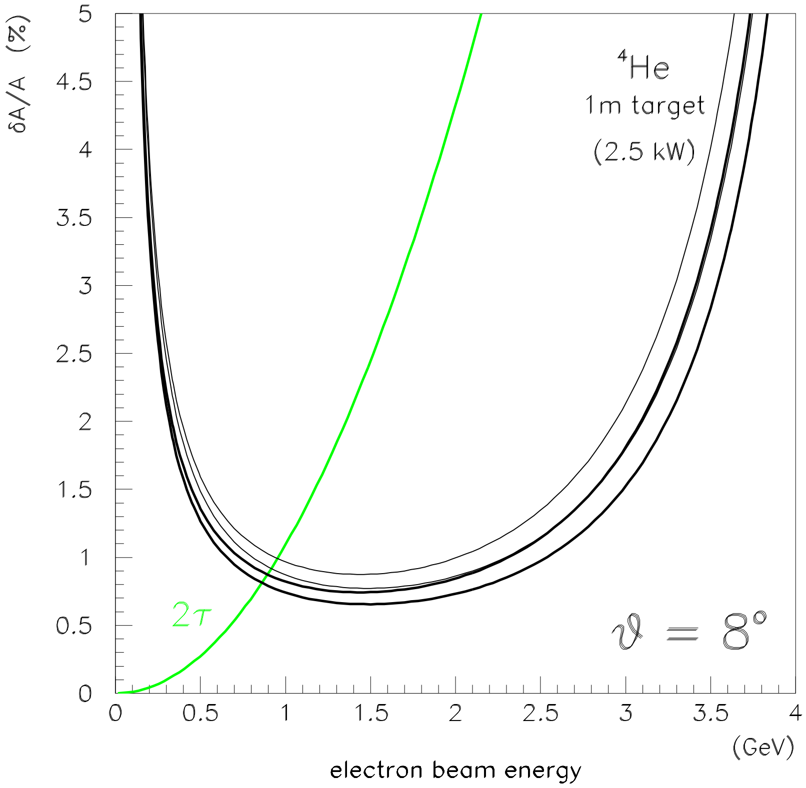

Figure 20: Percent uncertainty on measured asymmetry for a liquid helium target 1m in length with 100μA of electron beam and 8^o lab scattering angle. The curves come in pairs: two upper and two lower. Within each pair, the lower one assumes the full Mott cross section while the upper is includes only the counts which fall within $E_{\rm cut}$ = 20MeV of the elastic scattering peak. The upper pair of curves were calculated assuming a disk geometry for the target, so that scattered electrons traverse the full 1m before exiting the target. The lower curves result when a tube geometry is assumed, in which the scattered electrons exit the side of the target shortly downstream of the scattering event. A 20cm length of target was included in the latter case for the post-scatter target thickness to account for the lateral size of the tube and the target walls which must be traversed at an 8^o angle.

from the upstream region of the target, before the beam has begun to degrade due to radiation. The result is the lower pair of curves in Fig. 20, the upper (final) one of which largely overlaps with the lower curve of the "disk target" calculation.

6.3 multiple scattering

The two previous sections dealt with the scattering of the electrons from their nominal trajectory with respect to their energy. Along with this there will also be an accompanying scatter from the nominal trajectory with respect to direction. Multiple scattering arises mainly from Coulomb scattering from nuclei, both with and without accompanying bremsstrahlung. Besides the primary scattering event which provides the signal being measured, the electron suffers many small-angle deflections which add up to a total deflection angle distributed as a Gaussian with an r.m.s. given by

$$\theta_0 = \frac{0.0136\text{GeV}}{E}\sqrt{\lambda}\,(1 + 0.038\ln\lambda)$$

where λ is the target thickness in radiation lengths. From Fig. 3 it is clear that it is not sufficient to simply measure an asymmetry accurately, but one must also know with sufficient accuracy at what value of Q^2 it applies. For finite acceptance this involves an average over angles. In order to compare this average with a calculation one must know the shape of the envelope around the accepted angular range, which involves both the optics of the spectrometer and the smearing due to multiple scattering.

At 1GeV with a target thickness of 0.1 rad.len. the r.m.s. angular spread from multiple scattering is 3.9mr, or about 0.25^o. At 5^o Q^2 changes by 9% over 4mr, which implies the same rate of change for the asymmetry, and double for the cross section. At 8^o the figure is 6% for the asymmetry. Multiple scattering in the interior of the accepted angular region does affect the result, which involves only the sum of all counts within the acceptance. Hence the only thing of concern with regard to multiple scattering is its effect on the acceptance near the edges, with the low-angle extreme being the most sensitive.

The implications for alignment would be that the overall spectrometer angle would have to be known to within ± 0.1mr to ensure that geography would not contribute a significant amount to the total experimental error. With the proper placement and alignment of focal plane counters, it should not be a problem to reach the necessary precision with respect to angle, for a 1% measurement of the asymmetry.

7 Summary

The net effect of the corrections considered above is to decrease the effective luminosity, and hence statistical accuracy, of the measurement. The question then arises whether a systematic precision at the level of 10^{-9} is still needed, or whether 10^{-8} is sufficient. Fig. 21 shows the combination of the preceding two, but calculated for the case $S_A = 10^{-8}$. There is small but not insignificant decrement in precision that comes with this additional systematic error. But the major issue is that in order to address the important physics issues with such an experiment we need to reach the 1% level. Besides hoping to surmount the difficulties involved in operating a 2.5kW liquid-density helium target, there is another way to increase the statistical precision of the measurement, which is to run for a longer period of time. Since the combination of 100μA and 70% polarization is already a challenge to achieve over the duration of a 1000hr experiment, it is probably not wise to count on significant improvements in these values. In Fig. 22 is shown the measurement uncertainty for a 2000hr experiment under the same conditions as were assumed in Fig. 21.

Finally I repeat the calculation once again, substituting back a systematic error of 10^{-9}. The results are shown in Fig. 23. This probably comes close to the limit of what could reasonably be done in the near future at CEBAF. I would like to highlight the potential of an experiment with a helium target. A 1% measurement would be possible with a target of intermediate length between 12cm and 1m. Depending on the length of the target and how small the systematic errors can be made, a 1% measurement could be made at a single value of Q^2 in a 1000-2000hr experiment. If the experiment could not rely on prior knowledge of ρ_s at a sufficient level of precision, one could envision running at a pair of Q^2 points to the 1% level. While such an experiment would be quite difficult, it would yield a considerable variety of interesting physics, producing both a precise measurement of the strangeness radius of the nucleon and electroweak radiative corrections to

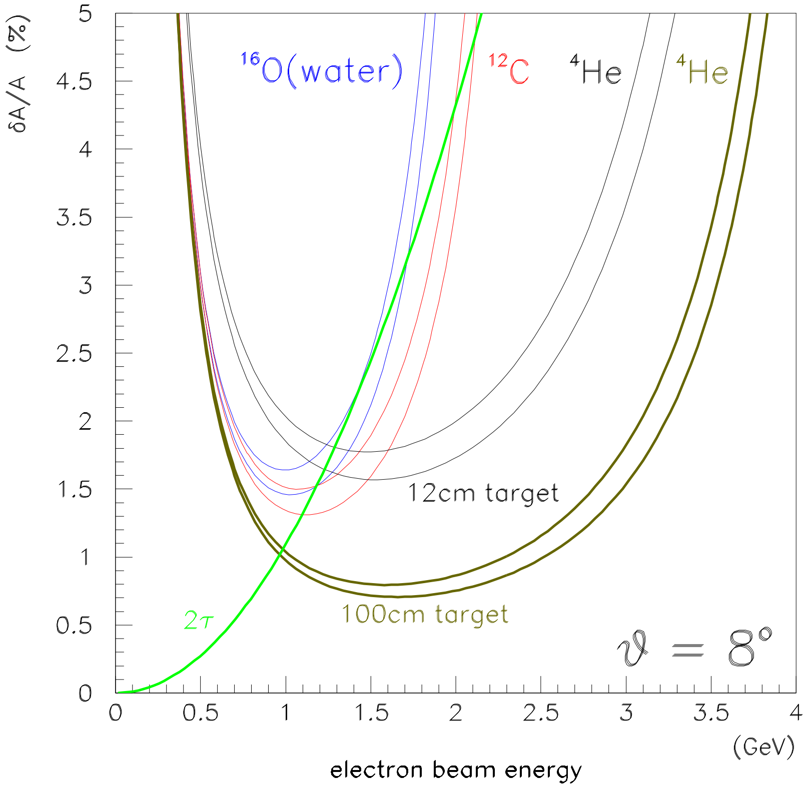

Figure 21: Percent error on the measured asymmetry *vs* electron beam energy fixed at 8^o lab scattering angle, after correcting for losses from external bremsstrahlung (lower curve of each pair) and both external and internal bremsstrahlung (upper curve of each pair). The Standard Model error arising from a ± 1 uncertainty in ρ_s is superimposed in green. A systematic error on the asymmetry of 10^{-8} has been assumed.

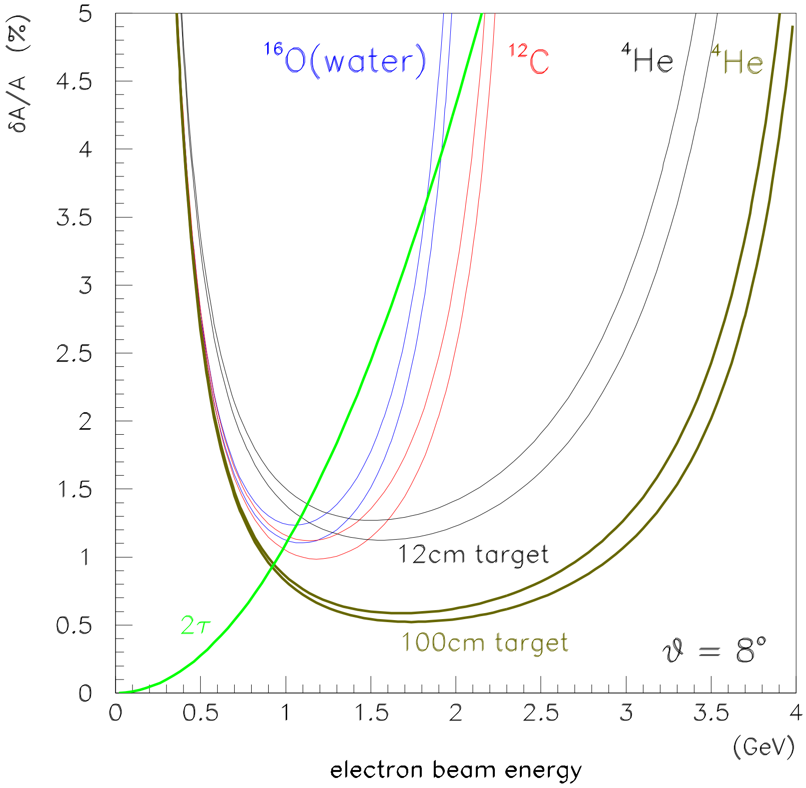

Figure 22: Same as Fig. 21, except for a 2000hr experiment instead of 1000hr. Systematic error on the asymmetry is kept at 10^{-8}.

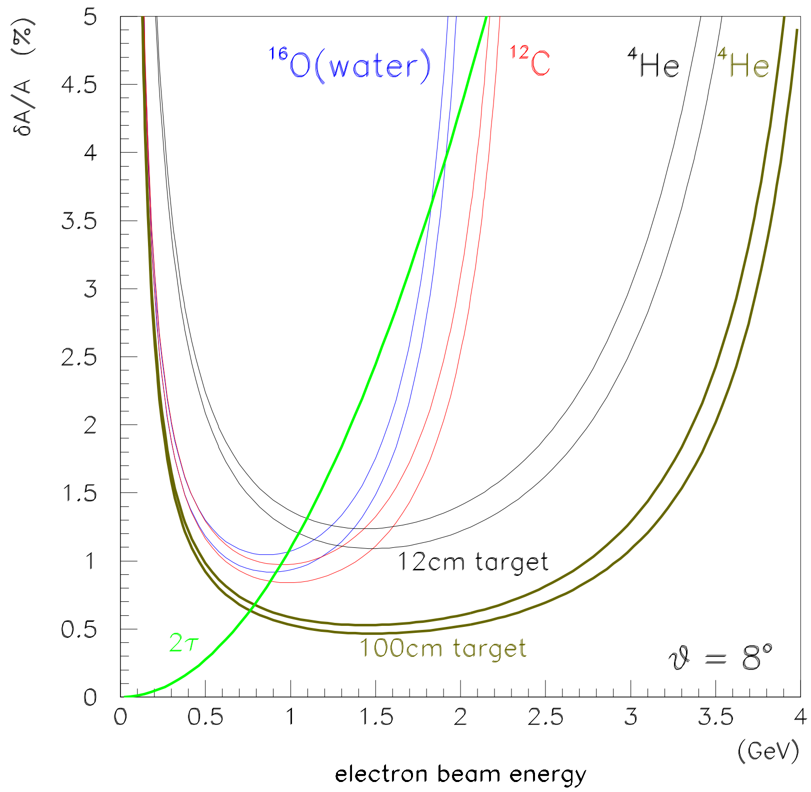

Figure 23: Same as Fig. 22, except for a systematic error S_A reduced to 10^{-9}.

lepton-quark scattering. I believe that the importance of these issues warrant the kind of effort that would be necessary to make an experiment of this type a reality.

Table 3: Beam heating power for a 100μA electron beam current, for various target materials.

	beam heating (W/cm)	target length (cm)	total power (W)
^{16}O (water)	200	3.6	720
^{12}C (graphite)	400	1.9	760
^{4}He (liquid)	24	113	2700
^{4}He (short)	24	12.5	300

A target heat dissipation

The ionization heating per unit length of a target is given by the product IS in W/cm where current I is measured in μA and stopping power S is measured in MeV/cm. The total power for the optimised targets discussed in the text of this report are shown in Table 3. Helium targets are not actually liquid phase, but rather cold gas under pressure. However they can have densities equal to or even slightly higher than that of liquid helium, so the difference is not important in calculating the thermal load.

A water target capable of dissipating 700W would have to be of the "waterfall" type. With the beam on the order of 1mm in diameter, the waterfall could be oriented so that it presents an edge to the beam. With this geometry the target could be quite thin in the transverse horizontal direction, which would reduce the effective amount of target seen by the average scattering electron, and hence reduce radiation losses somewhat. The graphite target is the simplest of all. In this case most of the heat dissipation takes place by blackbody radiation. If 700W is too much for a stationary target one could construct a rotating target. There is no apparent difficulty with carbon. With helium the amount of heating that could be handled by an affordable cryogenic system would be the limiting factor in what could be done. If a 15cm target can be made to operate successfully then several such targets could be arranged in series up to the desired length, limited by the total cooling capacity that could be put in place. Eventually there is also a limit imposed by the resolution of the spectrometer viewing an extended target, but at these forward angles I suspect that the cryogenic limits will be reached first. In Appendix B is described work that is presently underway to determine the experimental limits imposed by the spectrometer optics at forward angles.

B spectrometer resolution

The need for energy resolution at the level of a few MeV restricts the choices to one or two spectrometers among what is on the floor at CEBAF today. Fig. 24 taken from the Spring 1997 APS news bulletin, shows the energy spectrum for electron scattering from carbon with the HRS spectrometers in Hall A at kinematics not far from what we are presently considering. The 1MeV resolution is obtained using the full track-reconstruction capabilities of the spectrometer. The hardware resolution available for an integrating experiment of the type described in this report would be somewhat worse than this, perhaps by a factor of two, which is still sufficient for our purposes. The question remains whether this resolution can be maintained at angles forward of 10^o without sacrificing the solid-angle bite of 0.005sr per spectrometer.

Operation of the HRS pair at angles below 10^o will require the use of special septum magnets which adapt the spectrometer aperture for use at far-forward angles. At UConn we are in the process of setting up a simulation of particle trajectories inside the modified HRS spectrometers to determine the hardware resolution that can be obtained in this configuration. In this study we aim to determine what the trade-offs are between solid-angle, resolution, and far-forward acceptance for this spectrometer.

References

[1] M.J. Musolf, T.W. Donnelly, J. Dubach, S.J. Pollock, S. Kowalski, E.J. Beise, "Intermediate-energy Semileptonic Probes of the Hadronic Neutral Current", **Phys. Rept. 239**, pp.1-178, 1994.

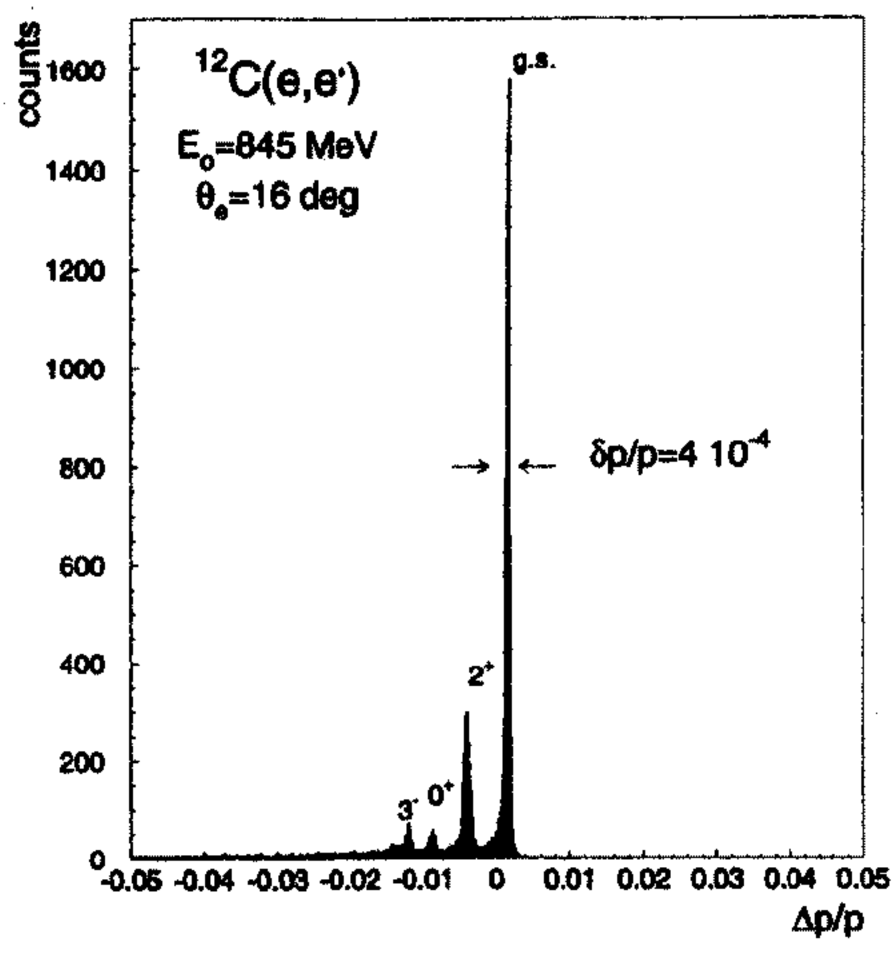

FIGURE 1. First $^{12}C(e, e')$ spectrum taken with one of the Hall A spectrometers at CEBAF (Ref. 1).

Figure 24: An experimental spectrum taken during one of the early Hall A experiments, showing the excellent resolution on the recoil electron energy that can be obtained with the HRS spectrometers. This figure was taken from the Spring 1997 APS news bulletin.